The ASKAP Roll Axis
Preliminary study of its benefits to calibration and imaging

Ian Heywood*, Aidan Hotan, David McConnell
CSIRO Astronomy & Space Science

Abstract

A standard test field containing numerous strong sources has been observed twice with the ASKAP BETA system, with the third axis of motion – the roll axis – disabled for the second run. These two data sets are subjected to identical calibration and imaging pipelines in order to gauge the effects of the roll axis when observing with a Phased Array Feed. Present beam forming techniques only allow meaningful comparisons to be performed with the on axis 'boresight' beam. Observing with the roll axis tracking reduces the standard deviation of the close-in imaging artefacts around the bright sources by factors of 2–3. Applying directional calibration techniques and examining the solutions reveals that the elevated artefacts are imparted by position and time dependent gain drifts with amplitude modulations of up to 50%, consistent with a rotating primary beam of non trivial shape.

*ian.heywood@csiro.au

1 Introduction

Telescopes with azimuth-elevation mounts experience a rotation between the coordinate frame defined by their aperture and that defined by the sky when tracking a celestial position. The Australian Square Kilometre Array Pathfinder (ASKAP) antennas are equipped with a third axis of motion – the roll axis [**1**] – that rotates the entire dish and feed structure as the observation progresses, tracking a fixed parallactic angle and thereby removing the apparent rotation of the sky. The presence of ASKAP's Phased Array Feed (PAF) system primarily motivated the inclusion of the additional rotation axis. Formed beams that are are maximally sensitive to directions away from the pointing axis of the dish can have fixed positions on the sky without having to be electronically steered via the continual updating of PAF element weights, and the instrumental polarisation response of the array is also expected to be significantly improved by maintaining a fixed parallactic angle.

This article presents an analysis of two observations conducted with the Boolardy Engineering Test Array [**2**]. Every effort was made to ensure that the observations were as similar as possible bar the fact that the roll axis was disabled for one of them. The goal is to determine the effect that the roll axis has on calibration and imaging. With the present beam forming techniques a comparison is only possible for a formed beam that is coincident with the pointing direction (a 'boresight' beam). As alluded to above, the off axis beams will move along circular loci with respect to the sky when the roll axis is disabled.

Section 2 describes the target field, the observations and the initial calibration steps. Discussion of the results of standard phase self calibration and the application and interpretation of differential (directional) gains are described in Sections 3 and 4, with concluding remarks in Section 5.

2 Observations and external calibration

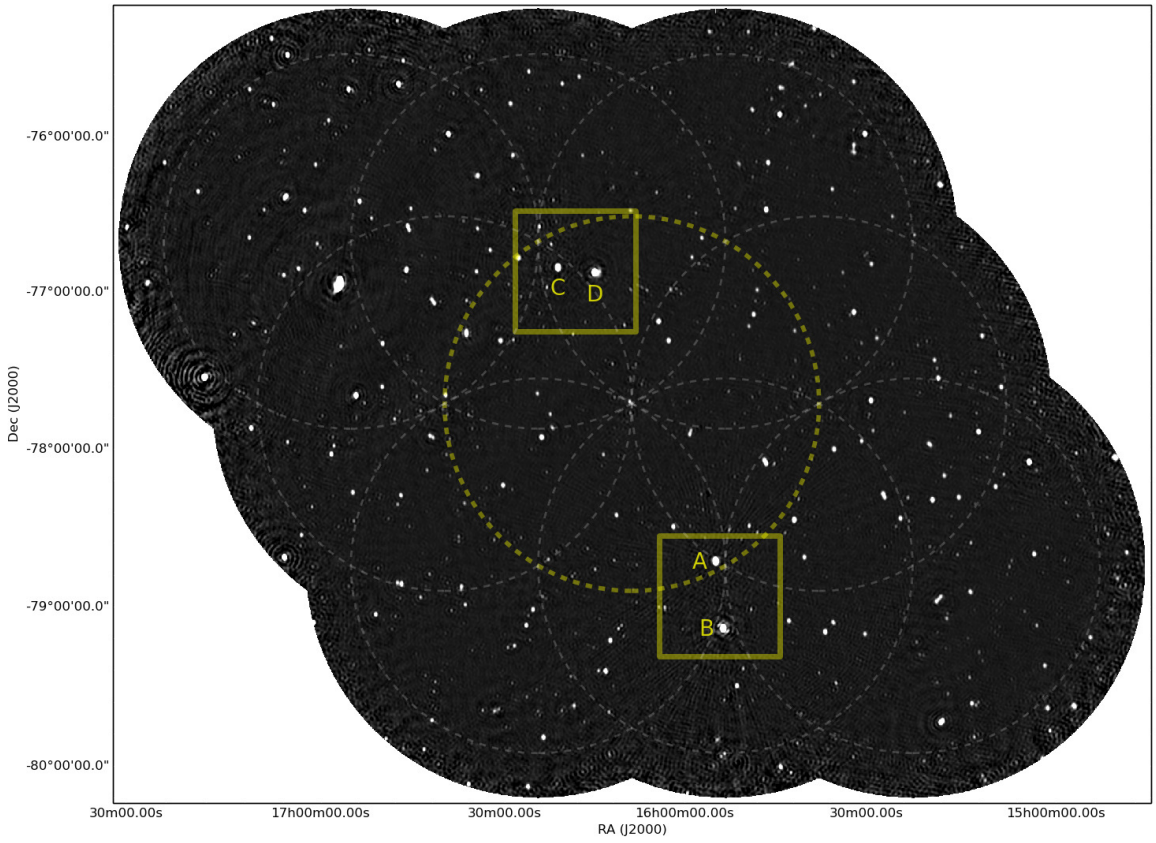

Figure 1: Nine beam image of the Apus field derived from the 'ON' observation. The greyscale is linear from -5 to 40 mJy beam^{-1}. The approximate half power point of the boresight beam (beam 0) is highlighted with the yellow dashed circle. In descending order of peak brightness the four dominant sources in the field are labelled A, B, C and D. The square regions are used for comparative residual measurements (see Section 3 and Figure 4).

The target field (the 'Apus' field, after the constellation in which it lies) contains a suitable arrangement of several strong sources. This and its proximity to the southern celestial pole mean it has become a standard

BETA test field, and was in fact the target for the first multibeam image produced with three ASKAP antennas [**3**].

The array tracked position RA = 16h 08m 52s, Dec = -78° 12m 06s (J2000) for a total of 19 hours (2 × 9.5 hours) on 10 August and 14 August 2014, with 711 to 1015 MHz of frequency coverage (Band 1) over 304 × 1 MHz channels. The only deliberate difference between the two observations was that on 10 August the roll axis was tracking as normal (the 'ON' observation) and on 14 August the roll axis was disabled (the 'OFF' observation). Nine formed beams were deployed in a standard mosaicking configuration, and the fully processed image from the 'ON' observation is shown in Figure 1. The *uv* coverages of the pair of observations can be seen in Figure 2. The only difference evident is the rotation caused by the sidereal time shifting between the observations.

The standard calibrator source B1934-638 is used for bandpass and flux scale calibration for each beam independently. The array is repointed such that B1934-638 is observed at the centre of each formed beam for ten minutes. Per-beam bandpass corrections in XX and YY are derived by averaging each of these scans in time and solving for corrections against a model [**4**]. The bandpass solutions are not normalised and therefore also encompass the flux scale calibration when applied to the relevant beams in the target field. A calibration run on B1934-638 was executed immediately prior to each of the two observations.

Following bandpass and flux scale calibration the target data are split into 8 × 38 MHz spectral windows, ready for self calibration. For a typical nine beam observation this results in 72 independent Measurement Sets, however for the roll axis experiment only beam 0 (the boresight beam) as indicated by the yellow circle on Figure 1 is considered. As mentioned in Section 1, off axis formed beams move on a circular track relative to the sky when the roll axis is disabled. While deliberately allowing this to occur can have certain practical applications for system diagnostic purposes, to correct for this in order to produce usable astronomical data would require the PAF element weights to be adjusted in real time.

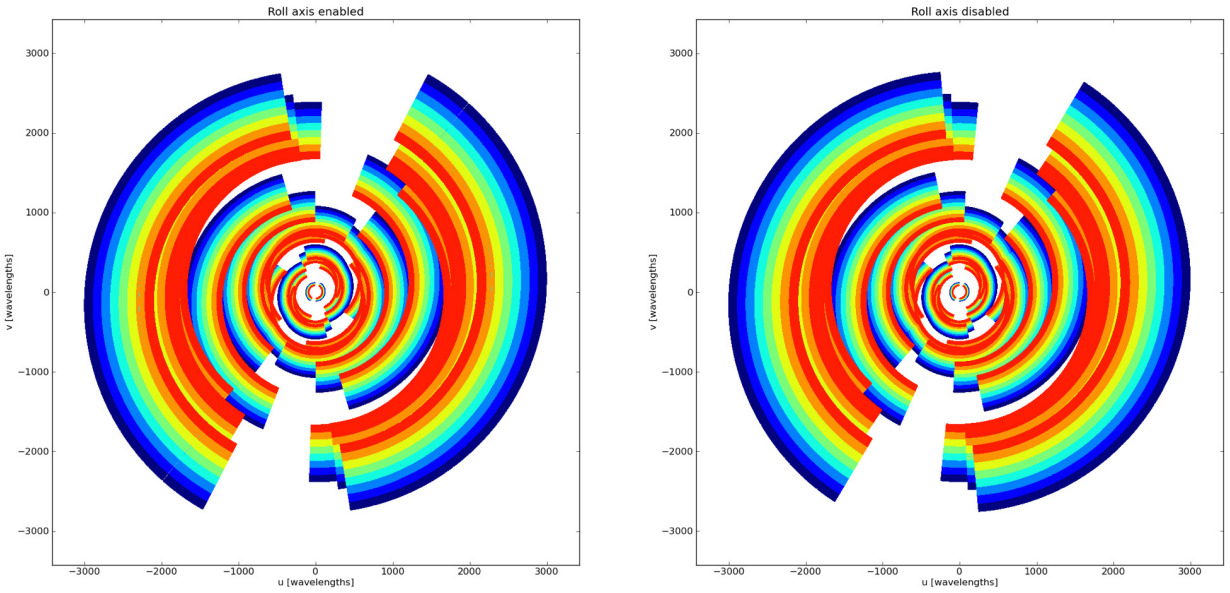

Figure 2: Fourier plane coverage of the 'ON' observation (left panel) and the 'OFF' observation (right panel). The colours represent the eight sub-bands into which the full 300 MHz of bandwidth is divided during calibration. With no calibrator visits and the RFI-free environment the coverage is complete for the full observation.

3 Self calibration

In the interests of subjecting the two observations to calibration and imaging steps that are as similar as possible an automated procedure is applied to beam 0 of both the 'ON' and the 'OFF' observations. The first step is to use CASA to image each of the eight spectral windows. These are subjected to a somewhat minimal cleaning operation (2000 iterations, unmasked) over an an area of 7.5 × 7.5 degrees, large enough to include sources detected through the primary beam sidelobes. A sky model is formed by using the PyBDSM [**5**] source finder to locate peaks of emission $>15\sigma$ in the resulting images, with Gaussian components fitted to extended sources. These models are visually examined for inclusion of artefacts. Phase only self calibration is then performed

using the MeqTrees package **[6,7]** against this model, deriving a single per-antenna phase-only correction for XX and YY for every two minutes of data, for every 8 MHz of bandwidth. Two data sets are then produced, namely a full set of corrected data, and a second corrected residual set with the sky model subtracted. These are re-imaged with the same shallow cleaning operation applied.

Figure 3 shows the images resulting from the uppermost of the eight spectral windows (977 - 1015 MHz) for both the 'ON' (blue frames) and the 'OFF' (red frames) observation. Image extents and colour scheme information can be found in the caption. The residual patterns around the strong sources are quantified in Figure 4. The lines show the pixel standard deviation values as measured from the dirty images formed from the residual visibility data, evaluated over the two regions (A-B and C-D) delineated by the yellow squares on Figure 1. The level of the close-in artefacts are typically a factor of >2 times higher in the 'OFF' observation than in the 'ON' observation, despite both observations being subjected to identical processing steps.

The effects on sources in the sidelobes of the primary beam is also important. A typical full track BETA observation (particularly in this frequency band) generally integrates for long enough for numerous sources to be detected through the close-in sidelobes of the primary beam, and if these sources are strong enough they must be included in the sky model for self calibration. Panels E and F in Figure 3 show two examples of such sources. The roll axis prevents apparent variability from being imparted to these sources due to the beam sidelobes washing over them as the observation progresses. Consequently they can be more readily deconvolved, or more accurately modelled during calibration.

Residual PSF sidelobe structures that do not deconvolve are typically due to deficiencies in the model of the instrument or the sky. The patterns associated with the strong sources in the 'OFF' image in Figure 3 are different from source to source; note the S-shapes (Figure 3, insets A and C) with varying orientations across the field. This is indicative of strong time and position dependent amplitude errors that cannot be removed by correcting a single complex gain term associated with each beam, i.e. by traditional self calibration methods. The Max-SNR method of forming beams does not constrain the beam shape in any way, thus ellipticity or other non-azimuthally symmetric structure in the main lobe of the primary beam is one possible explanation of this. Since the roll axis keeps the beam pattern static on the sky any azimuthally and radially dependent apparent variability imparted on the sources in the field is greatly suppressed. Any such structure in the beam can likely be removed as beam forming techniques mature to the point where the shape can be controlled, however with present methods the roll axis is clearly vital even for the boresight beam.

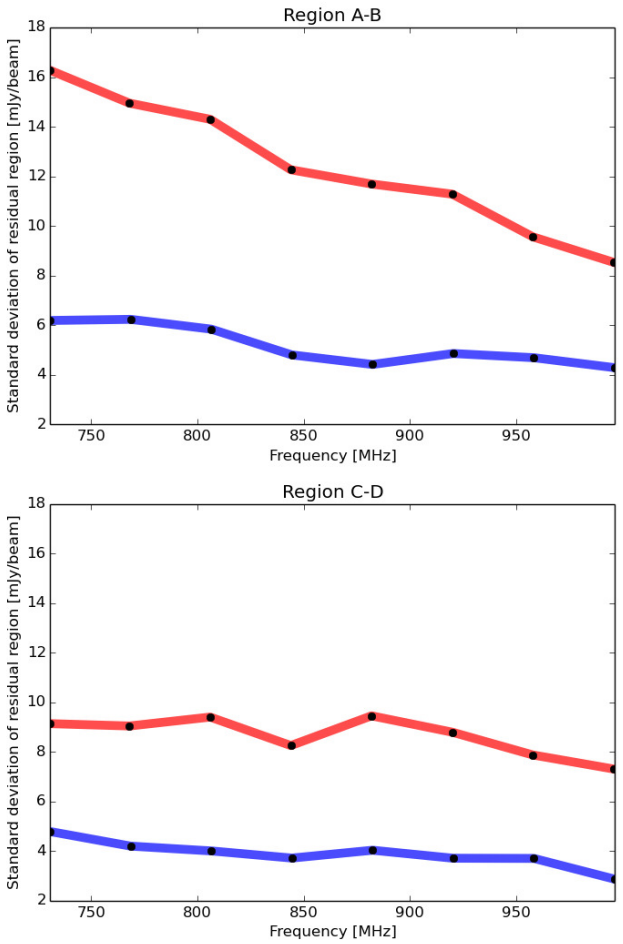

Figure 4: The measured standard deviations of the pixel values in the residual images as a function of frequency for the 'ON' observation (blue lines) and the 'OFF' observation (red lines). Measurements are made over the AB (upper panel) and CD (lower panel) regions as illustrated in Figure 1.

4 Differential gain solutions

The time and position dependent gains can be investigated further by means of directional calibration. In this case the differential gains technique **[8]** as implemented in MeqTrees is employed. Briefly, the instrumental model is expanded in order to include additional per-antenna solvable complex gain terms associated with the four bright sources. Phase and amplitude corrections are derived for these additional gain terms (in XX and YY) every 30 minutes and for every 4 MHz of data, whilst simultaneously fitting for the global phase corrections as described in Section 3. This technique can significantly improve the dynamic range of im-

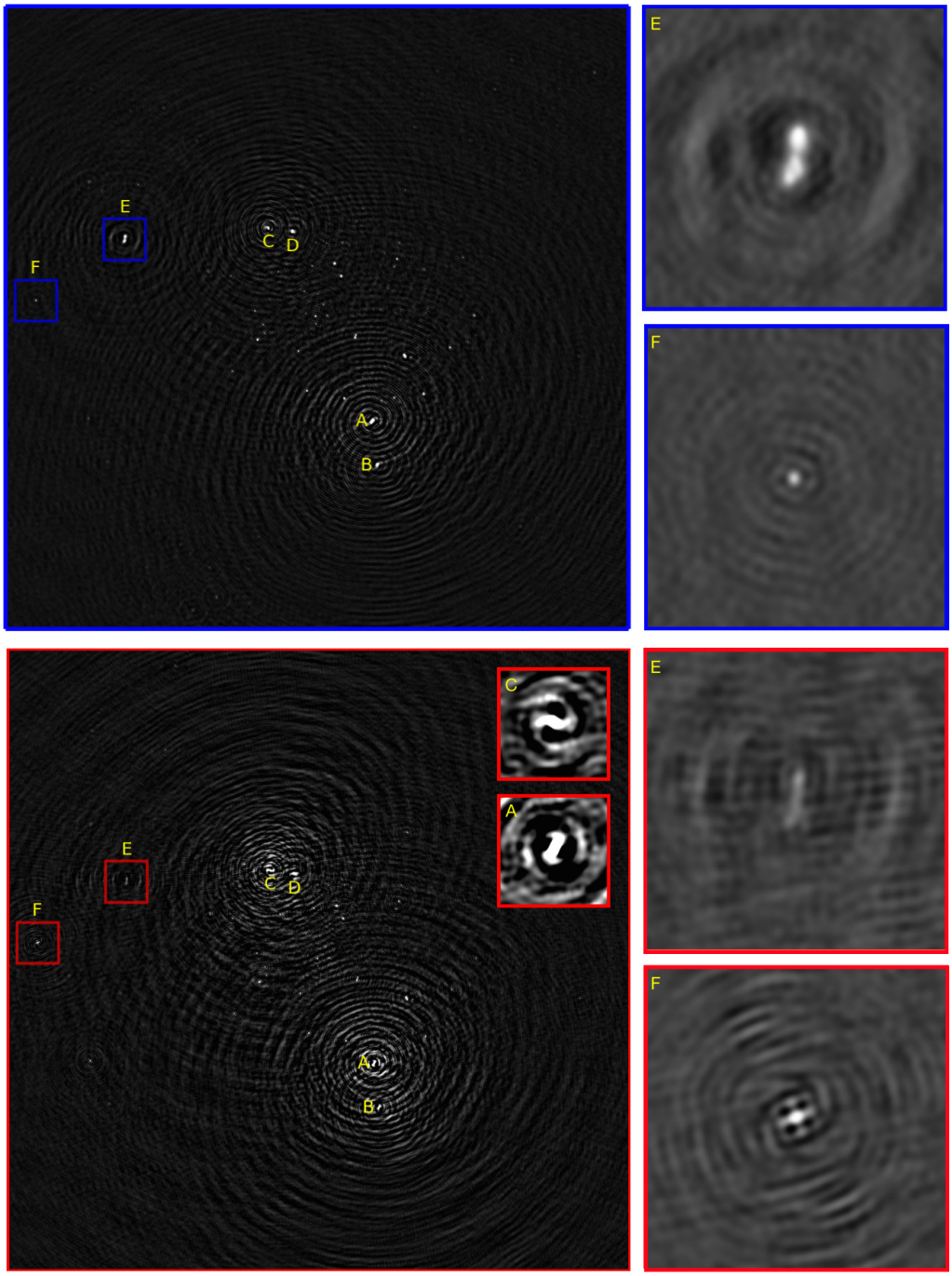

Figure 3: Images formed from the uppermost of the eight spectral windows (977 - 1015 MHz) using 2000 blind clean iterations for the 'ON' observation (blue frames) and the 'OFF' observation (red frames). The large panels span 6.3° with a linear greyscale that runs from -2 to 30 mJy beam^{-1}. The four dominant sources (ABCD) as per Figure 1 are marked, as are regions around sources E and F. The smaller panels show 25 × 25 arcminute zooms of these regions (linear grey scales running from -10 to 40 mJy beam^{-1}). The increased error patterns around the brightest sources when the roll axis is disabled are obvious, in particular how they vary from source to source (insets A and C, lower panel). Refer to the text for further details.

ages where tradition self calibration methods prove inadequate, but more importantly for the purposes of these observations, the gain solutions themselves encode much information about the behaviour of the instrument, the atmosphere or the sources themselves [**9,10**].

Figure 5 shows the normalised differential gain solution amplitudes, expressed as the mean of the values for all six antennas, for sources A, B, C and D (rows) and for the eight spectral windows (columns). Error bars represent the standard deviations of the solutions in the frequency domain. As usual the red and blue traces show the 'OFF' and 'ON' observations respectively.

The solutions are entirely consistent with the directional gains towards the four dominant sources being modulated in time by the rotation of an eccentric primary beam, or one where the true peak sensitivity is slightly off-axis. Amplitude corrections of up to 50% are required for the 'OFF' case. Note how the neighbouring source pairs (AB and CD) exhibit amplitude drifts that are qualitatively similar in time, with opposite magnitudes between pairs. For the 'ON' observation the differential gain amplitude corrections are much closer to unity, resulting in the much cleaner image derived from standard self calibration methods.

The blue points in Figure 5 show that the 'ON' observation is not completely free from time and position dependent primary beam effects. The likely cause of these are the slight known deficiencies in the array pointing model with regards to the azimuth and elevation directions, an issue currently being addressed by the commissioning teams.

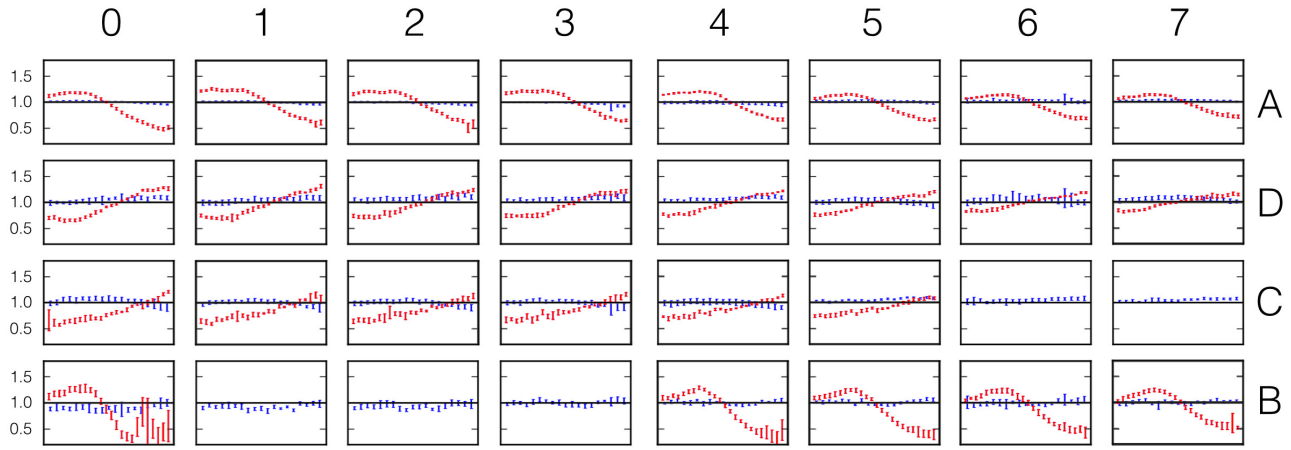

Figure 5: Per spectral window normalised differential gain amplitudes for sources A, B, C and D expressed as the mean value computed across all six antennas. The 'ON' observation in plotted in blue and the 'OFF' observation in red. Solutions are formed every 4 MHz and the error bars show the standard deviation of the solutions in the frequency intervals. The red dropouts seen for sources B and C occur when the source fails to meet the detection threshold used when automatically generating the sky models (likely due to the effects that are under investigation in this figure).

5 Conclusions

A pair of BETA observations, one with the roll axis disengaged, demonstrate that the roll axis is essential for successful observing using present beam forming techniques, even (contrary to what one might intuitively expect) in the case of the on-axis boresight beam. For the particular field observed for this study the measured standard deviations of the imaging artefacts present following phase self calibration are typically suppressed by a factor of 2 with the roll axis tracking. The application of differential gains to the bright sources in the field reveals that direction dependent primary beam effects are the primary cause of the imaging artefacts, modulating the amplitudes of sources by up to 50% when the roll axis is disabled.

Increasing the sophistication of beam forming methods for ASKAP is an on-going activity in the commissioning of the telescope, with the eventual goal being fine control over the shape and polarisation properties of the formed beam. In this eventuality the effects shown here that are caused by the disabled roll axis would likely be mitigated, however much more thorough understanding and control over the beam forming process will be required in order to observe with multiple beams with a two axis system.

This preliminary study shows the value of disabling the roll axis, as well as the use of astronomical sources and calibration to test the system, for example the use of differential gains to probe the beam shape. The imminent improvements to the BETA pointing model should be evident as a flattening of the blue points in Figure 5 in a repeat observation.

As beam forming techniques mature further 'ON/OFF' observations will prove informative. Of particular interest will be testing the effects of using the digital hardware to electronically and discretely steer off-axis beams, and the effect this has on imaging quality versus the smooth de-rotation of a static beam offered by the mechanical solution. The cost implications of the extra processing required, both in terms of electronically steering the beams and the more sophisticated calibration approach that may be required should also be quantified. This is an important consideration for the design of SKA Survey, and indeed all future PAF equipped interferometers.

Acknowledgements: IH thanks Oleg Smirnov for developing the software that was crucial to much of this analysis.

References

[**1**] Forsyth, R., et al., 2009, 11th Australian Symposium on Antennas, 30
[**2**] Hotan A., et al., 2014, PASA (preprint: arXiv 1409.1325H)
[**3**] `http://www.atnf.csiro.au/projects/askap/news_project_08042013.html`
[**4**] Reynolds, J., 1994, ATNF Technical Memos, 39.3/040
[**5**] `http://www.lofar.org/wiki/doku.php?id=public:user_software:pybdsm`
[**6**] Noordam, J. E., & Smirnov, O. M. 2010, A&A, 524, A61
[**7**] `http://www.meqtrees.net`
[**8**] Smirnov, O. M. 2011, A&A, 527, A107
[**9**] Smirnov, O. M. 2011, A&A, 527, A108
[**10**] Heywood, I., et al. 2013, MNRAS, 428, 935